Microphase-Separated Morphologies and Molecular Network Topologies in Multiblock Copolymer Gels

Mohammad O. Tuhin,[a] Justin J. Ryan,[b] J. David Sadler,[c] Zexiang Han,[d] Byeongdu Lee,[e] Steven D. Smith,[c] Melissa A. Pasquinelli[f*] and Richard J. Spontak[a,b,g*]

[a]Department of Chemical & Biomolecular Engineering, North Carolina State University, Raleigh, NC 27695, USA
[b]Department of Materials Science & Engineering, North Carolina State University, Raleigh, NC 27695, USA
[c]Corporate Research & Development, The Procter & Gamble Company, Cincinnati, OH 45224, USA
[d] Department of Materials, Imperial College London, London SW7 2AZ, UK
[e]Advanced Photon Source, Argonne National Laboratory, Argonne, IL 60439, USA
[f]Fiber & Polymer Science Program, North Carolina State University, Raleigh, NC 27695, USA
[g]IRIS Adlershof, Humboldt-Universität zu Berlin, Berlin 12489, Germany

ABSTRACT

Strong physical gels derived from thermoplastic elastomeric ABA triblock copolymers solvated with a midblock-selective oil continue to find use in increasingly diverse applications requiring highly elastic and mechanically robust soft materials with tunable properties. In this study, we first investigate the morphological characteristics of thermoplastic elastomer gels (TPEGs) derived from a homologous series of linear $A(BA)_n$ multiblock copolymers composed of styrene and hydrogenated isoprene repeat units and possessing comparable molecular weight, but varying in the number of B-blocks: 1 (triblock), 2 (pentablock) and 3 (heptablock). Small-angle X-ray scattering performed at ambient temperature confirms that (*i*) increasing hydrogenation reduces the microdomain periodicity of the neat copolymers and (*ii*) increasing the oil concentration of the TPEGs tends to swell the nanostructure (increasing the periodicity), but concurrently decrease the size of the styrenic micelles, to different extents depending on molecular architecture. Complementary dissipative particle dynamics simulations reveal the extent to which midblock bridging, which is primarily responsible for the elasticity in this class of materials, is influenced by both oil concentration and molecular architecture. Since constrained topological complexity increases with increasing block number, we introduce a midblock conformation index that facilitates systematic classification of the different topologies involved in nearest-micelle bridge formation. Those possessing at least one bridged and one looped midblock with no dangling ends are found to be the most predominant topologies in the pentablock and heptablock networks.

* To whom correspondence should be addressed (e-mail: melissa_pasquinelli@ncsu.edu or rich_spontak@ncsu.edu).

1. Introduction

Block copolymers continue to attract significant attention from the academic and industrial communities due principally to their intriguing ability to self-assemble into a wide range of soft nanostructures[1,2] that are precisely suitable for a diverse range of uses within the scope of a broad technological platform.[3-8] Due to the thermodynamic incompatibility between the covalently-linked blocks, these copolymers are capable of spontaneously self-organizing into several classical morphologies (*e.g.*, micelles on a body- or face-centered cubic lattice, cylinders on a hexagonal lattice or alternating lamellae), as well as more spatially complex morphologies (*e.g.*, double helices,[9] the gyroid,[10-12] the O^{70},[13,14] and the Frank-Kasper σ phase[15]). Of the many block copolymer archetypes that are commercially available, triblock copolymers that behave as thermoplastic elastomers[16] (TPEs) with hard (glassy or semicrystalline) endblocks and a soft (rubbery) midblock constitute an important and recyclable alternative to chemically cross-linked elastomers due to their ability to form a molecular network composed of bridged midblocks that physically connect neighboring microdomains (*cf.* **Figure 1**).[17] For this reason, they serve as soft materials capable of affording both scientific insight and application versatility through customizable properties, and independent experimental,[18-21] theoretical[22,23] and simulation[25,26] efforts focused on quantifying the fraction of bridged midblocks (υ) have been reported. Studies relating molecular arrangement to morphological and property development in bicomponent TPEs prepared from melt or solution processing are not, however, restricted to triblock copolymers, since both randomly-coupled[26-28] and perfectly-alternating[29-35] linear multiblock copolymers have also been synthesized and investigated in this broad copolymer family.

In the same fashion as a parent homopolymer,[37-39] incorporation of a selective solvent into an ordered block copolymer can elicit several responses, including microdomain swelling, one or

more order-order transitions or microdomain dissolution at the order-disorder transition. These responses depend on the thermodynamic incompatibility of the copolymer, the copolymer concentration and temperature. Experimental studies[40] of midblock-solvated triblock copolymers with and without an endblock-selective additive verify that these systems exhibit the same phase behavior observed[41] with selectively-solvated diblock copolymers. A recent simulation investigation[41] of midblock-solvated triblock copolymers furthermore indicate that unique morphologies, such as the truncated octahedron, can likewise develop. In the specific case of triblock copolymer TPEs, addition of a midblock-selective diluent such as a nonpolar oligomeric oil yields tunably compliant thermoplastic elastomer gels (TPEGs) for use as dielectric[43-47] and phase-change[48-50] elastomers, pressure-sensitive adhesives,[51] and substrates for microfluidics[52] and flextronics.[53] This paradigm naturally extends to include polar diluents such as water[54] and ionic liquids[55] in the case of triblock or higher-order multiblock copolymers possessing hydrophobic endblocks and a hydrophilic midblock. These functional soft materials are of interest in the fabrication of proteinaceous hydrogels,[56] Li-ion batteries,[57] soft robotics,[58] organic photovoltaics,[59,60] and water-treatment[61,62] or amphoteric gas-separation[63] membranes. An especially attractive attribute of TPEGs is their ability to be (electro)mechanically strain-cycled with little, if any, hysteresis.[64] Moreover, these materials are capable of avoiding dynamic fatigue and achieving ultrahigh elongations, with some reaching strains of ≈4000% prior to failure.[65]

The illustration provided in **Figure 1** displays rigid micelles that are responsible for connecting swollen soft midblocks and thus stabilizing the molecular network in conventional TPEGs. In the case of TPEGs derived from ABA triblock copolymers, a single copolymer molecule can at most physically connect two micelles. In the case of $A(BA)_n$ multiblock

copolymers with n > 1, however, a single molecule can form multiple bridges and connect up to n+1 micelles. While previous studies of TPEGs have focused primarily on triblock copolymers, the objective of this study is to elucidate the morphological characteristics and constrained chain topologies responsible for network formation in TPEGs composed of multiblock copolymers. In this spirit, we have synthesized a homologous series of perfectly-alternating linear multiblock copolymers with constant molecular weight (M), and investigated their morphologies as functions of copolymer architecture and solvent concentration by small-angle X-ray scattering (SAXS). In addition, dissipative particle dynamics (DPD) simulations have been performed to identify the molecular conformations responsible for soft-midblock bridging and, hence, network formation. Due to the topological complexity introduced with multiblock copolymers, a conformation-based classification index is proposed and used to compare the relative influence of all nearest-micelle bridge conformations.

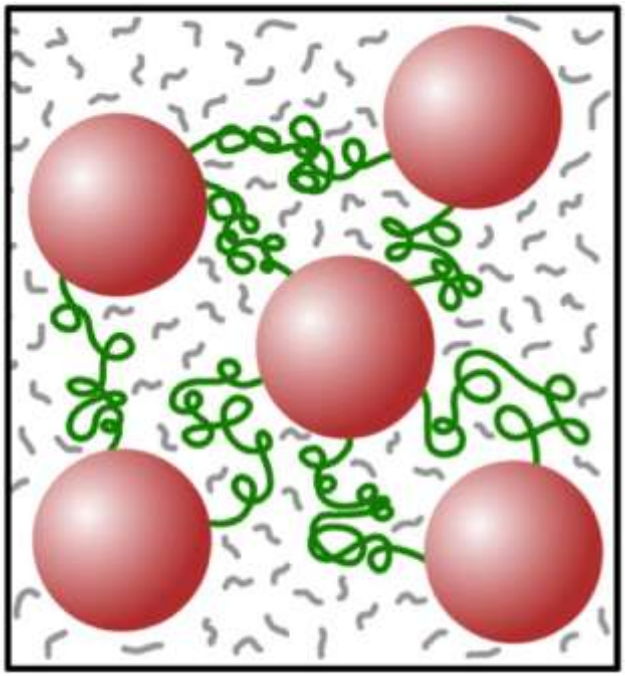

Figure 1. Illustration depicting the rigid micelles (red) that serve as physical crosslinks in TPEGs. $A(BA)_n$ multiblock copolymers can possess up to n soft-block bridges (green) that are selectively swollen by the added diluent (gray) and physically connect up to n+1 micelles.

2. Experimental

A. Materials

For the synthesis of the three model multiblock copolymers, cyclohexane (HPLC grade) was

obtained from VWR, whereas isoprene and styrene were supplied by Aldrich. Both the cyclohexane and isoprene were used as-received, but the styrene required purification to remove by-products. This was achieved by first degassing the styrene with N_2, followed by titration with dibutylmagnesium (Aldrich) to a yellow end point and then column chromatography. In addition to *sec*-butyllithium (Aldrich), Irganox-1010 (Ciba-Geigy) and ultrahigh-purity hydrogen (Matheson), methanol, 2,3-dimethyl-3-pentanol (DMP), nickel(II) bis(2-ethylhexanoate), triethyl aluminum (1 M solution in heptane), hydrochloric acid (HCl), and sodium bicarbonate ($NaHCO_3$) were purchased from Aldrich and used as-received. The diluent was a primarily aliphatic mineral oil (MO, Hydrobrite 380, Sonneborn). Copolymers consisting of styrenic (S) endblocks and 1-3 isoprenic (I) midblocks separated by S blocks (with $M_{S,midblock} = 2M_{S,endblock}$ to account for the extension difference between an endblock tail and a midblock bridge/loop) were synthesized in the presence of *sec*-butyllithium and cyclohexane at 60°C by living anionic polymerization.[32] The composition of each copolymer was fixed at 20 wt% S, and the number-average M and polydispersity (Đ) values ranged from 293 to 303 kDa and 1.05 to 1.14, respectively, as determined by size-exclusion chromatography and ^{1}H NMR spectroscopy (performed on a GE QE-300 spectrometer), respectively. Copolymer designations (including I midblock number and block masses, in kDa) are as follows: TBC (n = 1, $S_{30}I_{240}S_{30}$), PBC (n = 2, $S_{15}I_{120}S_{30}I_{120}S_{15}$) and HBC (n = 3, $S_{10}I_{80}S_{20}I_{80}S_{20}I_{80}S_{10}$). Polyisoprene (PI) in all copolymers was 95-99% hydrogenated to yield ethylene-*alt*-propylene (EP) rubber, as described elsewhere.[66]

B. Methods

The copolymers were co-dissolved with the mineral oil as the EP-selective midblock diluent, ranging in solvent weight percent (ϕ_S) from 0 to 96%, and 1.0 wt% Irganox 1010 in reagent-

grade toluene at a solution concentration of 4% w/v. Resultant solutions were cast into Teflon molds and dried for 8-9 days at ambient temperature to yield films measuring 1.2-1.5 mm thick. These films were heated to 120°C for 6 h under vacuum, quiescently cooled for 12 h, carefully removed from the molds and wrapped in Al foil, and then stored in a plastic container at ambient temperature and pressure until testing. Subsequent SAXS analysis was conducted at ambient temperature on beam-line 12-ID-B at the Advanced Photon Source (Argonne National Laboratory). The sample-to-detector distance and beam spot size were 2 m and 0.5 x 0.025 mm^2, respectively, and the 14 keV beam provided a wavelength (λ) of 0.087 nm and a flux of ~10^{12} photons/s. Two-dimensional SAXS patterns collected on a 2-D Pilatus 2M detector were azimuthally integrated to yield intensity profiles expressed as a function of the scattering vector (q), where $q = (4\pi/\lambda)\sin\theta$ and θ is half the scattering angle.

3. Simulations

The DPD simulations performed here conform to the procedures previously detailed,[25] and we provide an abbreviated overview below. Since the coarse-grained beads in DPD simulations behave as soft (compressible) spheres, they can remain discrete in the case of diluent molecules or they can be linked together to mimic polymer chains as bead-spring equivalents. Each bead is coarse-grained to 1 kDa, and so the ~300 kDa copolymer chains described above correspond to 300 beads, where a single A bead represents ~10 S repeat units and a B bead accounts for ~14 EP repeat units. Since the molecular weight of the MO is ~0.5 kDa, one solvent bead accounts for ~2 solvent molecules. The net force ($\mathbf{f}_i$) that bead i (i = A, B or S) experiences at position $\mathbf{r}_i$ is expressed as the summation of all forces accounting for pairwise interactions with all other (j) beads within a characteristic radius (R_C) typically set to unity, and is written as

$$\mathbf{f}_i = \sum_{j \neq i} (\mathbf{F}_{ij}^C + \mathbf{F}_{ij}^D + \mathbf{F}_{ij}^R + \mathbf{F}_{ij}^S) \quad (1)$$

where $\mathbf{F}_{ij}^C$ represents the conservative (repulsive) force given by

$$\mathbf{F}_{ij}^C = \begin{cases} a_{ij}\left(1 - \frac{r_{ij}}{R_C}\right)\hat{r}_{ij} & \text{for } (r_{ij} < R_C) \\ 0 & \text{for } (r_{ij} > R_C) \end{cases}, \quad (2)$$

and α_{ij} corresponds to the pair-repulsion potential between beads i and j, $\hat{\mathbf{r}}_{ij} = \mathbf{r}_{ij}/|\mathbf{r}_{ij}|$, and $r_{ij} = |\mathbf{r}_{ij}|$ is the scalar distance between beads. The spring force ($\mathbf{F}_{ij}^S$) only exists between connected beads comprising the polymer chains and is represented by $-k_s(r_{ij} - r_0)\,\hat{\mathbf{r}}_{ij}$, where $k_s = 4.0$ and $r_0 = 0.8$. The dissipative ($\mathbf{F}_{ij}^D$) and random ($\mathbf{F}_{ij}^R$) forces in Eq. 1 retain their usual meanings, and values of the various parameters and number bead density ($\rho = 3$) required in these terms are selected to ensure consistency with prior DPD studies[67] of block copolymers. Similarly, the like pair-repulsion parameters (α_{AA}, α_{BB} and α_{SS}) are calculated from 75 kT/ρ, where k is the Boltzmann constant and T denotes absolute temperature (kT = 1 at a system thermostat set equal to 373 K so that $\alpha_{AA} = \alpha_{BB} = \alpha_{SS} = 25$). We presume that the solvent is B-selective so that $\alpha_{BS} = \alpha_{BB}$. In contrast, the value of the unlike pair-repulsion parameters involving A (α_{AB} and α_{AS}) are determined[68] from $\alpha_{AA} + 3.27(1 + 3.9/N^{0.51})\chi$, where N is the number of beads per chain and χ is the Flory-Huggins interaction parameter estimated from the solubility parameters for PS and EP.

The DPD simulations were performed with the Large-scale Atomic/Molecular Massively Parallel Simulator (LAMMPS) software package[68] under the conditions of a microcanonical ensemble to ensure constant mass, volume and energy so that the total number of beads representing both solvent and copolymer molecules was held constant in a cubic cell measuring 23 R_c on each side to ensure that at least 100 copolymer chains would be in the most dilute system. The *chain.py* routine was used to build the copolymer chains and to distribute them

randomly with the solvent beads in the simulation box. Each system was then equilibrated up to 5×10^5 steps with a time step of 0.05 and periodic boundary conditions using *nve* integrator. It is important to note here that doubling the cell size or reducing the time step (to 0.02 or 0.04) did not generate any statistically different results. Production runs, on the other hand, were performed for an additional 5×10^5 steps. All simulations were performed on the Henry2 cluster at the NC State High Performance Computing Center. The discrete microdomains of neat $A(BA)_n$ copolymers and their selectively-swollen gels were systematically identified from snapshots of the simulation trajectories using a versatile density-based clustering algorithm (DBSCAN),[69] which does not presume a particular microdomain shape *a priori;* its application to

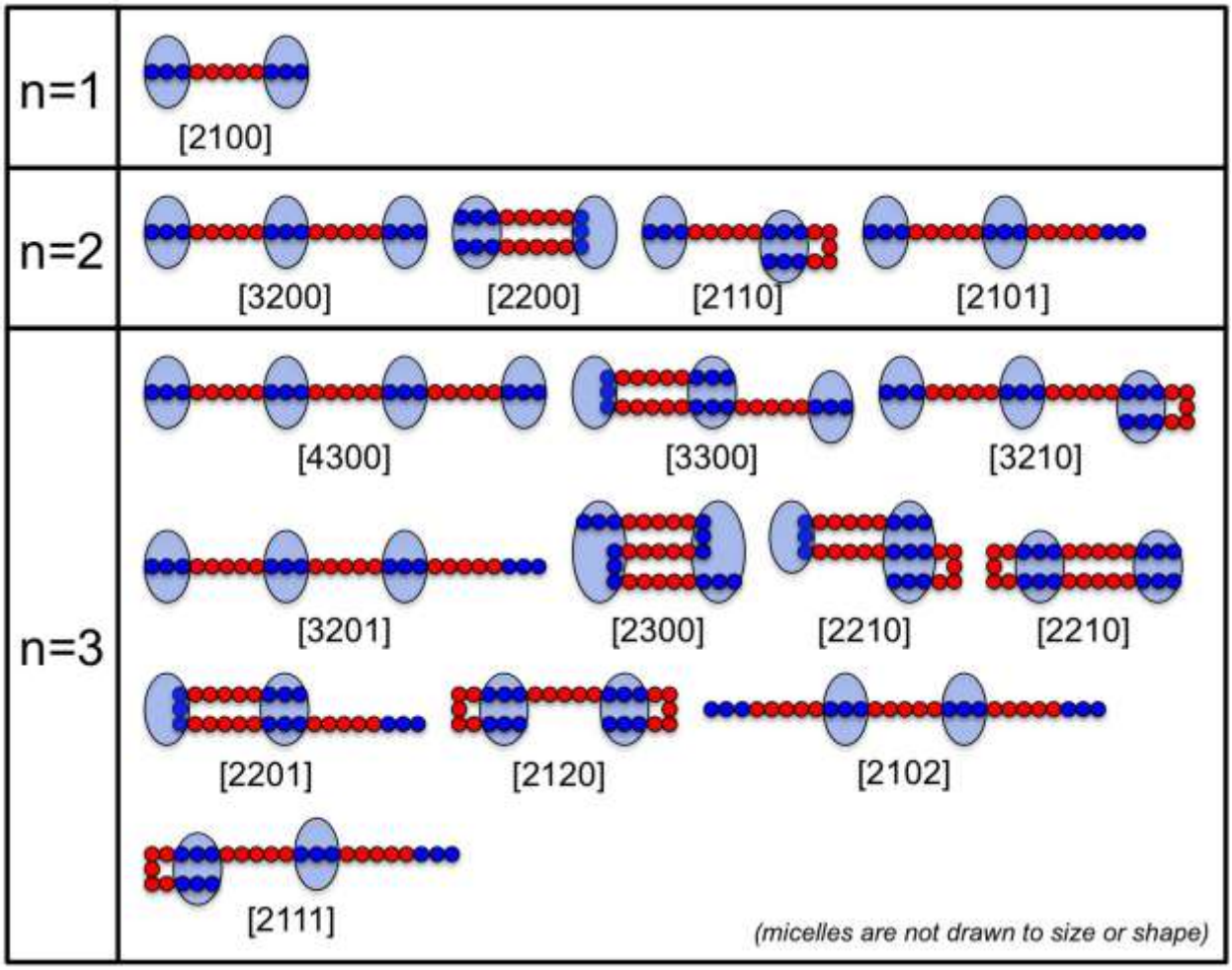

Figure 2. Schematic diagram of the various molecular conformations responsible for networks composed of linear $A(BA)_n$ multiblock copolymers varying in the number of swollen soft-midblocks (n, red): 1 (TBC), 2 (PBC) and 3 (HBC). Rigid blocks (dark blue) are able to self-organize into micelles (light blue), and the only conformations considered here possess soft-midblocks that bridge nearest-neighbor micelles. Corresponding MCI designations of the form [#micelles, #bridges, #loops, #dangles] are included for each conformation that connects at least 2 micelles and confirm that little degeneracy exists up to n=3.

particle simulation trajectories has been described elsewhere.[25] We adapted DBSCAN, which employs the *flexible procedures for clustering* (fpc) package within the R statistical software suite, to be used in conjunction with an in-house algorithm so that periodic boundary conditions could be considered when counting midblock conformations. Constrained topologies identified for each $A(BA)_n$ chain by the existence of nearest-neighbor soft-midblock bridges were classified here according to a midblock conformation index (MCI) of the form [mbld], where m is the number of connected micelles, and b, l and d represent the number of B bridges, B loops and A dangling ends, respectively. Schematic illustrations and corresponding MCI designations of conformations encountered for TBCs (n=1), PBCs (n=2) and HBCs (n=3) are presented in **Figure 2** and reveal that the level of topological complexity quickly increases with increasing n.

4. Results and Discussion

A. Morphological Characteristics

Neat Copolymers

Since the multiblock copolymers initially consist of isoprenic midblocks, we first examine the neat (diluent-free) copolymers to ascertain the effects of molecular architecture (n) and hydrogenation on morphology at constant M. The corresponding SAXS profiles are provided in **Figure 3** and confirm that the 3 copolymers are microphase-ordered, displaying a well-defined principal peak at q* and at least two higher-order reflections. Although the peaks are quite broad, the position of the second-order peak (at q_2) relative to q* varies from 1.76 to 1.82, suggesting that the morphology consists of S cylinders or spheroids poorly arranged on a hexagonal lattice

(for which $q_2/q^*=1.72$) in a continuous EP-rich matrix. At the constant copolymer composition (20 wt% S), however, spheroidal or ellipsoidal micelles are more intuitively expected. Important considerations that might be responsible for the results displayed in **Figure 3** include the copolymer molecular weight coupled with a large chemical difference between the block species and the multiblock architectures. The first two factors contribute to a high thermodynamic incompatibility (χN) and slow diffusion, while the third results in a downward shift and flattening of the ordered block copolymer envelope as n is increased, according to self-consistent field theory predictions.[70] Thus, under the current experimental conditions, a polydisperse spheroidal morphology is reasonable and moreover consistent with the scattering results included (and modeled in terms of the form factor) in **Figure 4**. The apparent shift in the form factor to higher q with increasing n indicates that the micelles become smaller, which is a direct consequence of increasing n at constant M. Two additional observations included in the inset of **Figure 3** indicate that the microdomain periodicity ($D = 2\pi/q^*$) decreases with increasing n and with increasing hydrogenation. The first finding is attributed to the reduction in block sizes associated with increasing n, and can, in the strong-segregation limit, be described by $D \sim (n + 1)^{-2/3}$. Soft-midblock hydrogenation,

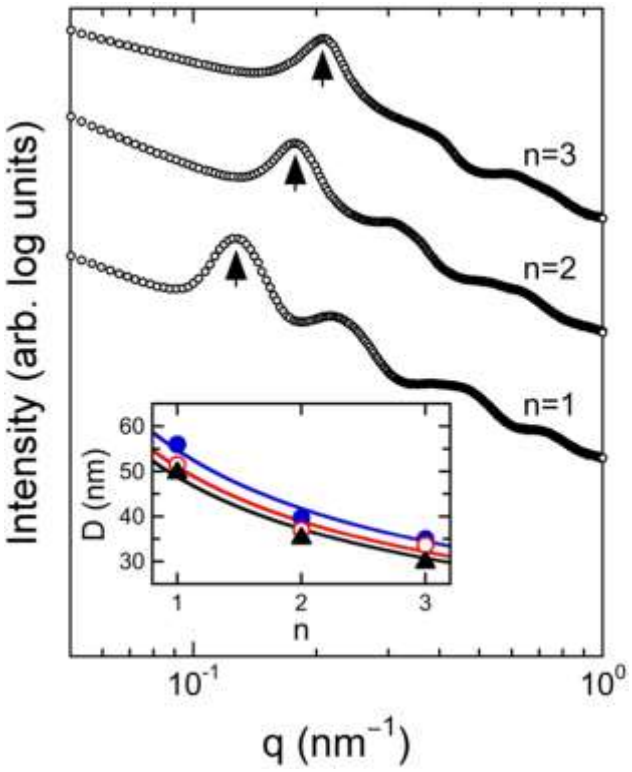

Figure 3. SAXS intensity profiles measured from neat multiblock copolymers varying in n (labeled). Each arrow identifies the principal peak at q*. In the inset, D (=2π/q*) is included as a function of n for all three copolymers at different degrees of hydrogenation (in mol%): 0 (blue), 50 (red) and ≈97 (black). The color-coded lines correspond to the scaling relation in the text.

which serves to increase χN, likewise promotes a marginal reduction in D at constant n. This result is, however, contrary to that predicted from strong-segregation theory,[71] as well as

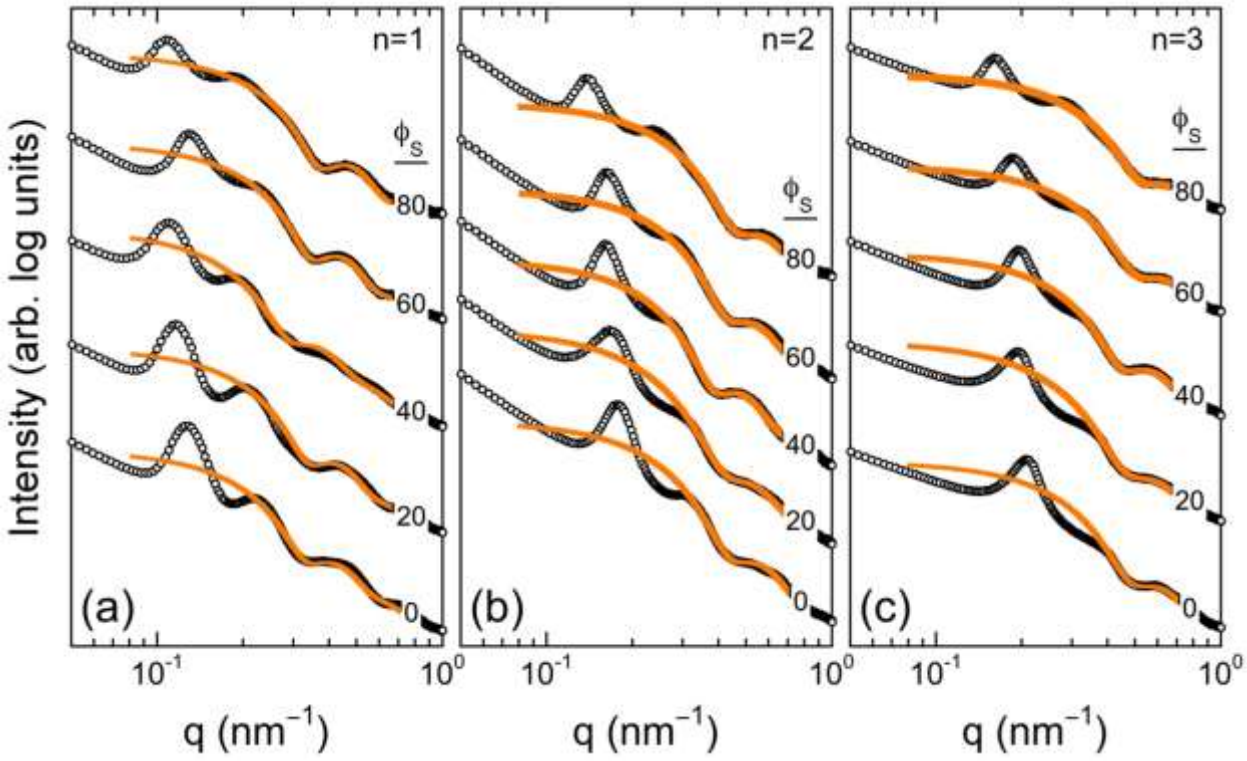

Figure 4. SAXS profiles acquired from TPEGs varying in molecular architecture (n) — (a) 1, (b) 2 and (c) 3 — at different ϕ_S (labeled, in %). The position of the second peak relative to q* suggests that all of these systems possess hexagonal close-packed S spheres. The curve fits (gold) correspond to the form factor for polydisperse spheres.

experimentally reported,[66] for unconstrained (*i.e.*, non-networked) diblock copolymers and clearly warrants further investigation.

Swollen Copolymers

Three series of SAXS profiles acquired from TPEGs varying in ϕ_S from 0 to 80% in 20% increments are presented in **Figure 4** for

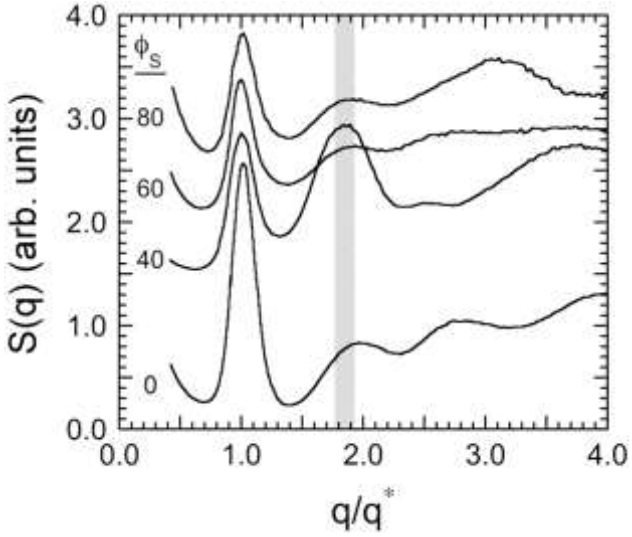

Figure 5. Structure factor, S(q), values extracted from the SAXS data in **Figure 4** for several swollen TPEGs varying in ϕ_S (labeled, in %) with n=1, and vertically shifted to facilitate viewing. The shaded region identifies the range of the second maximum, confirming that the spherical morphologies are not bcc or fcc.

oil-swollen multiblock copolymers differing in molecular architecture: n=1 (TBC, **Figure**

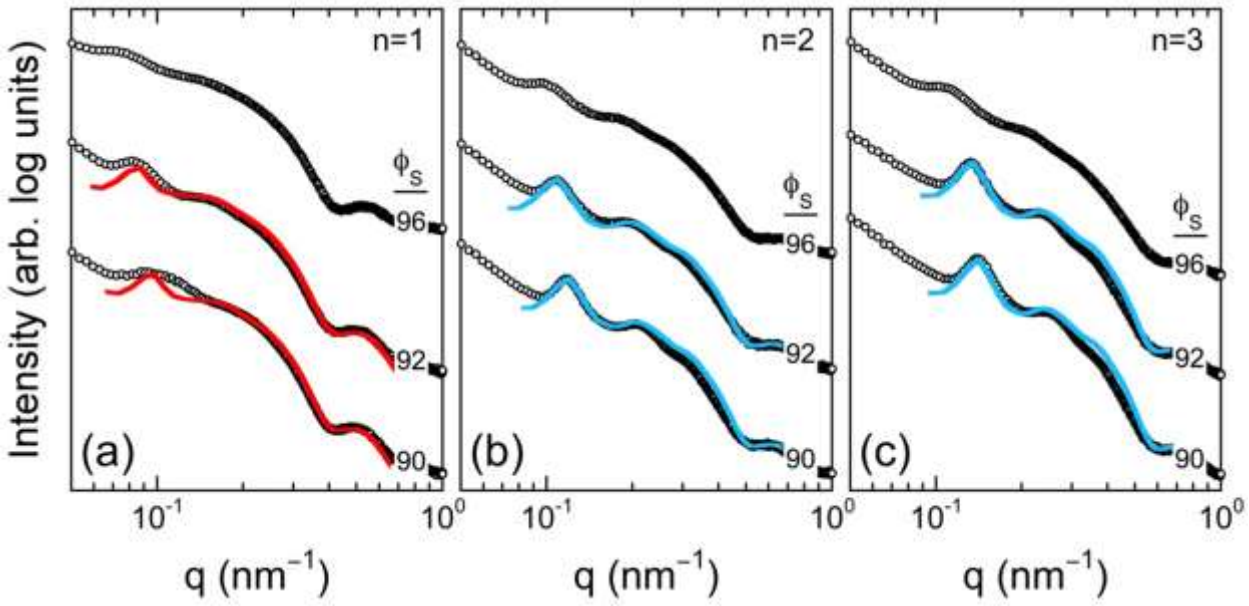

Figure 6. SAXS profiles measured from TPEGs varying in molecular architecture (n) — (a) 1, (b) 2 and (c) 3 — at different ϕ_S (labeled, in %). The position of the second peak relative to q* indicates that the PBC- and HBC-based TPEGs possess hexagonal close-packed S spheres in an oil-swollen EP matrix up to ϕ_S=92%. The red and blue curves represent model fits for hexagonal close-packed and 2D hexagonal spheres, respectively.

4a), n=2 (PBC, **Figure 4b**) and n=3 (HBC, **Figure 4c**). The model fits included in **Figure 4** represent the form factor for polydisperse spheres and favorably match the SAXS data at moderate to high q. In all of the cases examined, an ordered morphology reminiscent of that in the neat copolymers remains discernible, in agreement with previous[72,73] examples of TPEGs. Most prior studies of TPEGs composed of styrenic triblock copolymers with either an EP or ethylene-*co*-butylene (EB) midblock and aliphatic mineral oil possess a body-centered-cubic (bcc) spherical morphology,[74] although the face-centered-cubic (fcc) morphology has likewise been reported for block copolymers.[40,75,76] The relative signature peak positions (expressed as q_2/q^*) of the SAXS profiles in **Figure 4** signify that a hexagonal-close packed morphology persists in all the TPEGs considered. Mean values of q_2/q^* are 1.76 ± 0.01 for n=1 (**Figure 4a**), 1.74 ± 0.02 for n=2 (**Figure 4b**) and 1.76 ± 0.02 for n=3 (**Figure 4c**). Values of the structure

factor, S(q), extracted[77] from the triblock copolymer and several associated TPEGs are provided as a function of q normalized with respect to q* in **Figure 5** and, despite the broad scattering peaks, confirms that the spherical micelles are not arranged on a bcc or fcc lattice. At higher ϕ_S (90% and above), the TPEGs approach their critical gel fraction below which the population of copolymer molecules becomes insufficient to form a molecular network. Detailed examination of this regime by dynamic rheology and mesoscale simulations reveals[78] that the critical gel fraction is sensitive to copolymer attributes such as molecular weight, composition and architecture. In **Figure 6**, long-range order appears lost when $\phi_S > 90\%$ in the case of n=1 (**Figure 6a**), but is retained for the remaining two copolymers up to $\phi_S = 92\%$ at least in **Figures 6b** ($q_2/q^*=1.76$ for n=2) and **6c** ($q_2/q^*=1.78$ for n=3) even though the block masses become smaller with increasing n. Model fits corresponding to hexagonal close-packed and 2D hexagonal spheres are included in **Figure 6** and verify that the spheres are loosely positioned on a hexagonal lattice with relatively short-range order (no distinction is made here between the two lattice types). We do not discount the possibility of fcc ordering since this

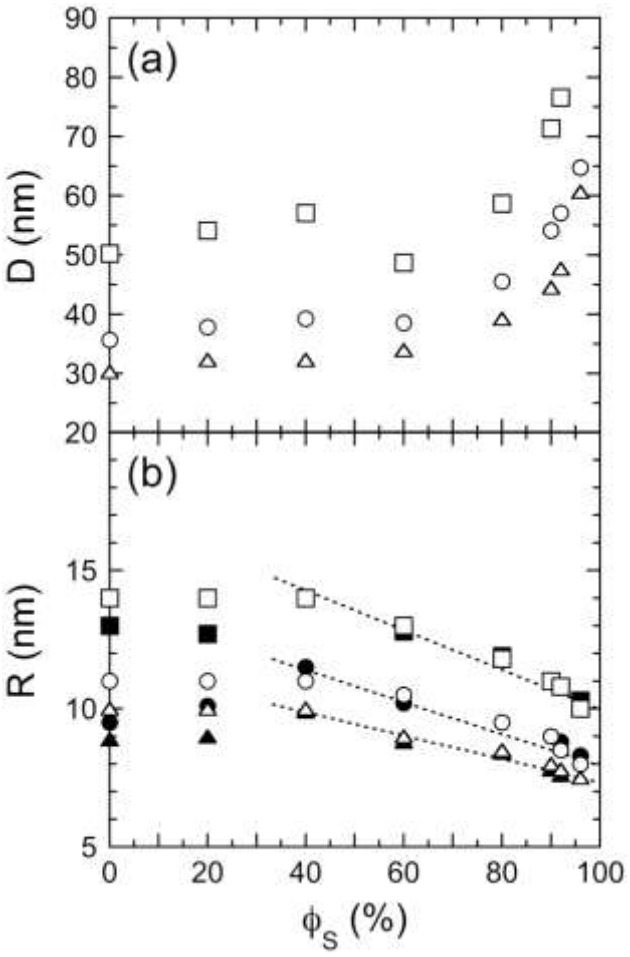

Figure 7. Values of (a) D and (b) R extracted from SAXS profiles for TPEGs varying in copolymer architecture (n) — 1 (squares), 2 (circles) and 3 (triangles) — as a function of ϕ_S. In (b), the open and filled symbols correspond to monodisperse and polydisperse spheres, respectively. The dotted lines in (b) serve as guides for the eye and indicate the range over which R decreases nearly linearly upon matrix swelling.

lattice with numerous stacking faults and non-correlated {111} planes yields broad second peaks and resembles the 2D hexagonal arrangement.

Two important nanostructural dimensions extracted from the SAXS profiles provided in **Figures 4** and **6** are the periodicity (D) and spherical radius (R), which are included as functions of ϕ_S and n in **Figures 7a** and **7b**, respectively. On one hand, as anticipated from the results presented in **Figure 3** for the neat copolymers and the fact that the block masses systematically decrease with increasing n at constant N, D consistently decreases with increasing n over the entire range of ϕ_S examined in **Figure 7a**. For each copolymer series, an increase in ϕ_S from 0 to ~60% generally promotes a modest (10-14%) increase in D. Above 60% oil, however, D increases sharply (by as much as ~100% relative to the neat copolymer in the case of the HBC series). Values of R have been modeled as both monodisperse and polydisperse spherical micelles from the form factor at intermediate q values (model fits for polydisperse spheres are included in **Figure 4**) and are displayed in **Figure 7b**. Although R expectedly decreases with increasing n due to the accompanying change in block mass (estimated values of the unperturbed gyration diameter for the S blocks in the neat TBC, PBC and HBC specimens are 9.7, 6.9 and 5.6 nm, respectively), it is sensitive to polydispersity below ϕ_S = 40%. At and beyond this dilution level, R appears to depend less on polydispersity and decrease monotonically with increasing ϕ_S. The results included in **Figure 7** reveal that the S-rich microdomains become not only more separated (from D) but also physically smaller (from R) as ϕ_S increases. Volume-fraction estimates derived from R and D confirm that the S micelles are spherical and not cylindrical. Corresponding values of D/R for monodisperse spheres up to ϕ_S = 60% average 3.5 ± 0.1 over all n. At higher ϕ_S, D/R more than doubles to 8.1. In the next section, we use DPD simulations to determine if changes in TPEG morphology influence the midblock conformations responsible for

network formation.

B. Conformational Analysis

To begin, final snapshots collected from equilibrated DPD simulation trajectories representing multiblock-based TPEGs with n = {1, 2, 3}, each collected at 4 different values of ϕ_S, are portrayed for comparison in **Figure 8**. Three important features of these results warrant

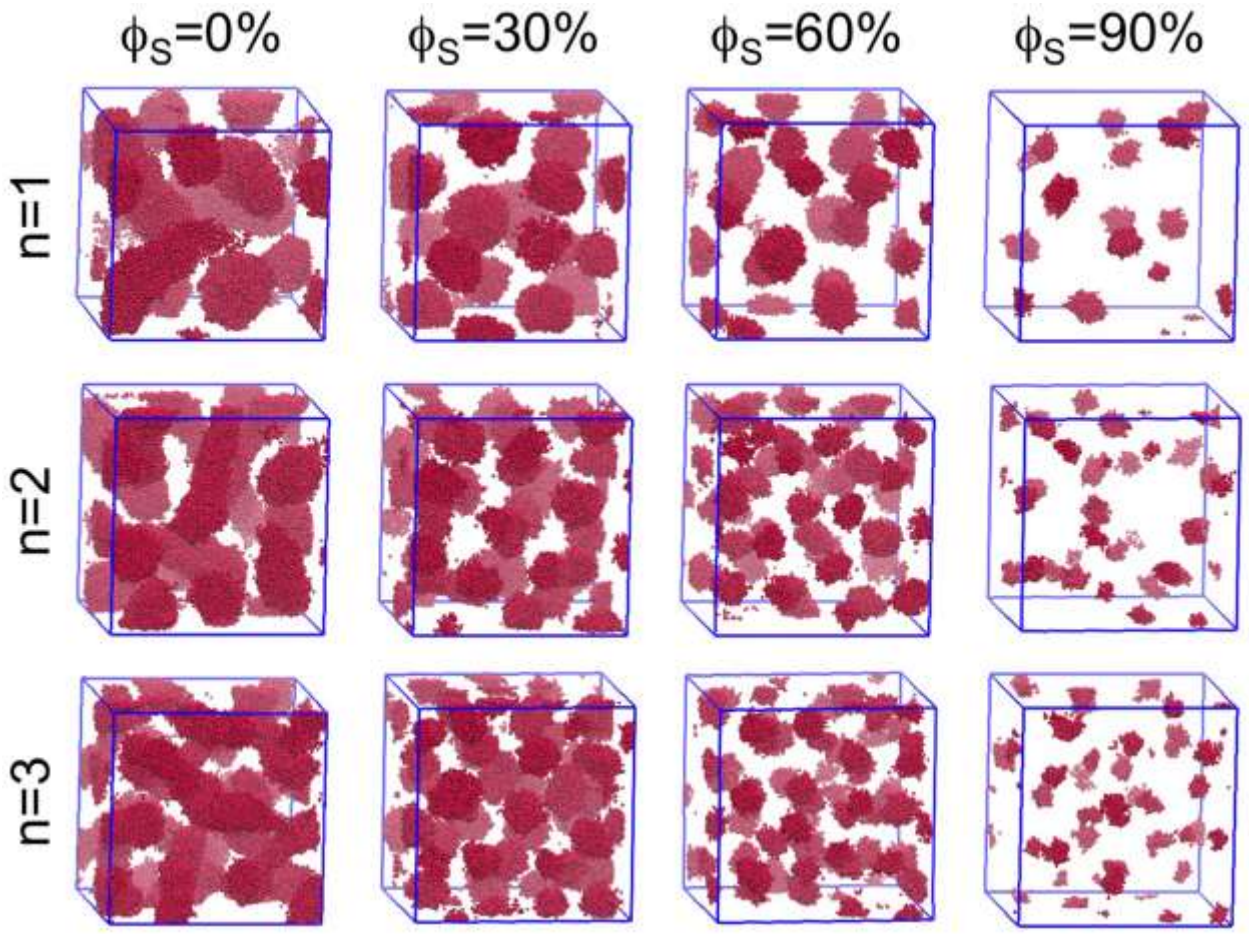

Figure 8. Equilibrated DPD simulation trajectory snapshots acquired from selectively-solvated linear multiblock copolymers varying in molecular architecture (n) and solvent content (ϕ_S), as labeled.

discussion at this juncture. First, in the solvent-free systems (ϕ_S = 0%), the discrete micro-domains visible in **Figure 8** appear elongated, which is consistent with the existence of distorted spheres. As ϕ_S is increased, however, most of the microdomains become less elongated and more

spherical in shape. This observation supports the conclusion based on the SAXS form factor analyses in **Figure 4** that the micelles in these TPEGs are spheroidal. Second, the microdomains in the simulations do not possess obvious evidence of long-range order, as implied by the SAXS data. Third, an increase in ϕ_S is accompanied by an increase in separation distance (which relates to D) and a reduction in microdomain size (which relates to R). Corresponding values of D/R are 3.3 ± 0.1 over all ϕ_S and n. Thus, we conclude that the DPD simulations capture several, but not all, of the important characteristics of the TPEGs investigated in this study. The most likely reason for differences is either the length required for each bead to be coarse-grained to 1 kDa or the total number of chains, as each simulation was conducted with 100-1000 copolymer chains, excluding the solvent beads. Once the simulations are run beyond equilibration and the micro-domains are subsequently identified by the DBSCAN cluster algorithm, individual chain conformations are analyzed and organized according to the MCI classifications described earlier.

Before discussing the chain topologies derived from DPD simulations, the MCI classification scheme proposed here is examined on the basis of its two assumptions and potential drawbacks. The first assumption is that at least two micelles must be connected by a single copolymer chain so that a network can form. Since the index requires the number of connected micelles (m), we note that $m_{min}=2$, thereby precluding consideration of single micelles with

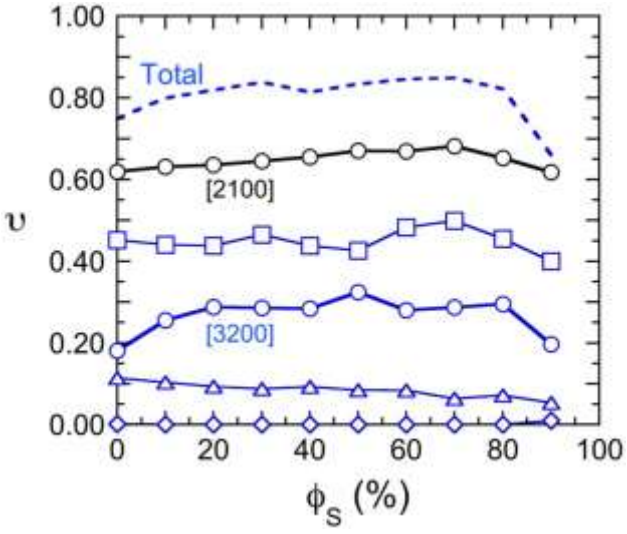

Figure 9. Values of the bridging fraction (υ) presented as a function of ϕ_S for selectively-solvated TBCs (black) and PBCs (blue). MCI designations include [2200] (Λ), [2110] (□) and [2101] (◇). Solid lines serve to connect the data, and bold lines identify the fully extended conformations with $m=m_{max}$. The dashed line is the total bridging fraction obtained by summing all the individual conformational contributions.

numerous loops or dangling ends. Since b_{max}=n for a fully extended chain occupying the maximum number of micelles possible, m_{max}=n+1 at the opposite extreme. The second assumption is that only chain conformations responsible for connecting nearest-neighbor micelles are considered. As an example of a conformation that would not be included, consider an extended ABABA PBC molecule similar to the one classified as [3200] in **Figure 2**. If the A midblock is not contained within a micelle (and behaves as a dangling midblock), then m=2 and the two A endblocks would ultimately immobilize the entire chain but at a much lower crosslink density than the other PBC conformations. In the spirit of chemically-crosslinked elastomers, the conformations included in the MCI classification scheme require that the molecular mass between physical crosslinks (*i.e.*, the rigid micelles) must equal the mass of the soft midblocks. Another consideration to be addressed regarding the proposed MCI scheme is degeneracy; that is, the possibility that a given designation corresponds to more than one conformation. An example of such degeneracy is the [2210] conformation for n=3 included in **Figure 2**. Insofar as we are aware, this is the only case of degeneracy in all the cases examined here. While the extent to which degeneracy occurs is expected to increase further with n > 3, we elect to combine results obtained for conformations assigned to the same MCI.

The fraction of copolymer bridges ascertained from DPD simulations of TBC- and PBC-based TPEGs analogous to the experimental analogs is provided as functions of ϕ_S and MCI designation in **Figure 9**. In the case of the TBC materials with n=1, only one conformation classified as [2100] contributes to network formation (*cf.* **Figure 2**). It is important to recognize that all other conformations are taken into account to extract each value of υ furnished in this section. Results provided for the TBC-based TPEGs are numerically comparable to those reported[42,77] elsewhere from both DPD and Monte Carlo simulations. In the case of TPEGs

derived from PBCs (with n=2), the four conformations illustrated in **Figure 2** must be analyzed. The fully extended conformation connecting the maximum number of micelles (m_{max}=3) is designated as [3200] and accounts for about 20-30% of all conformations. Interestingly, υ associated with the [2110] conformation connecting two micelles and possessing one B-midblock bridge and one B-midblock loop ranges from 40 to 50% over the entire range of ϕ_S examined. In marked contrast, the most compact topology ([2200]) only contributes 5-10%, whereas the [2101] designation, constituting the only conformation with a thermodynamically unfavorable dangling end, is negligible, adding only 0-1%. The total bridging fraction afforded by PBC-based TPEGs, obtained by summing the results from all the individual MCI designations, is ≈85%, which is considerably higher than the maximum υ (≈68%) afforded by TBC-based TPEGs due to the greater topological complexity inherent in PBCs.

The substantial increase in topological complexity in TPEGs derived from HBCs is immediately evident from **Figure 10** wherein conformations responsible for connecting 4 (the maximum number possible) or 3 micelles are displayed in **Figure 10a** and

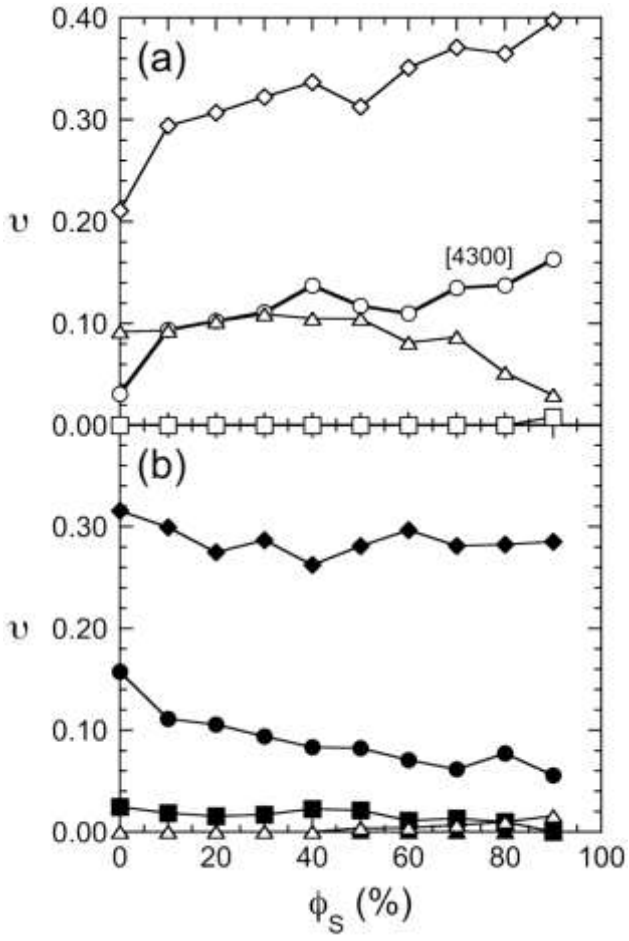

Figure 10. Values of υ as a function of ϕ_S for selectively-solvated HBCs in which m = 3 or 4 in (a) or m = 2 in (b). MCI designations in (a) include [3300] (⩚), [3210] (◇) and [3201] (□). Those in (b) include [2300] (■), [2210] (●), [2201] (▲), [2120] (◆), and [2111] (⩚). Solid lines serve to connect the data, and the bold line identifies the fully extended conformation with m=m_{max}.

those connecting only 2 micelles (the minimum number considered) are included in **Figure 10b**. Although υ corresponding to the fully extended [4300] conformation appears to increase with increasing ϕ_S, it is important to recognize that this conformation at most accounts for ≈16% of all possible topologies. Values of υ for the alternative, less extended conformation that likewise possesses 3 B-midblock bridges/molecule, designated as [3300], remain comparable to those of the [4300] conformation up to $\phi_S \approx 50\%$ and then decrease as ϕ_S is increased further. The dominant conformation visible in **Figure 10a** is designated as [3210], as it connects 3 micelles with 2 B-midblock bridges and possesses a single B-midblock loop. In this case, υ increases from about 21 to 40% as ϕ_S is increased from 0 to 90%. As with the PBC-based TPEGs in **Figure 9**, values of υ determined for the counterpart to this conformation with a dangling end instead of a B-midblock loop ([3201]) are insignificant (<1%). In **Figure 10b**, the highly deleterious effects (responsible for low υ) of one or two dangling ends (*i.e.*, the [2201] and [2111] topologies or the [2102] topology, respectively) and compaction (*i.e.*, the [2300] topology) are apparent. While the most prominent conformation connecting 2 micelles and possessing a nearly constant bridging fraction (≈29%) is designated as [2120] with 1 B-midblock bridge and 2 B-midblock loops, its analog described as having 2 bridges and 1 loop ([2210]) provides a more modest contribution that generally decreases monotonically from 16% in the neat copolymer to about 6% when $\phi_S = 90\%$. Upon summing all the values of υ in **Figure 10** for HBC-based TPEGs, over 90% of the copolymer molecules are found to participate in network development via B-midblock bridging.

5. Conclusions

In this study, we have investigated the morphological characteristics and chain topologies of

TPEGs composed of linear multiblock copolymers custom-synthesized by living anionic polymerization to possess comparable composition and molecular weight but different molecular architecture, and selectively hydrogenated from PI to EP. According to analysis of the form factor in SAXS profiles, the morphologies of the neat and solvated copolymers are generally classified as spheroidal, which agrees with results from accompanying DPD simulations. From the relative scattering peak positions, 2D or 3D hexagonal close-packed spheres appear to persist as the copolymers are solvated up to 92% in the case of the PBC- and HBC-containing systems. These findings will be compared to transmission electron microscopy results in a forthcoming publication. As the TPEGs become increasingly solvated, the microdomain periodicity initially increases slowly and then sharply at relatively high solvent levels (> 80%). Corresponding spherical radii extracted from scattering form factors are sensitive to polydispersity at low ϕ_S (< 40%) and then become nearly monodisperse (and decrease nearly linearly) at high ϕ_S. By introducing a midblock conformation index (MCI) as a means by which to develop a molecular-level classification scheme of the network,[79,80] we can systematically categorize the various molecular conformations that contribute to network formation in these TPEGs. Since topological complexity increases significantly with an increase in the number of blocks along the copolymer backbone, this index is anticipated to augment existing theoretical treatments[81,82] of block copolymer self-assembly and network formation in solution. In the cases of the PBC- and HBC-based systems, the likelihood of chains being fully extended so as to connect the maximum number of micelles possible is less than that of chains possessing at least one swollen midblock loop. Since these copolymer molecules are highly incompatible, conformations with a dangling endblock are negligible. The objective of this study is to elucidate the nanostructural characteristics and detailed chain topologies of TPEGs derived from linear multiblock

copolymers so that conformation-structure-property relationships can be developed in this remarkably versatile and tunable class of soft and elastic materials.

6. Acknowledgments

This work was supported by the NC State Nonwovens Institute and DFG Grant EXC 1027 Bild Wissen Gestaltung. This research used resources of the Advanced Photon Source, a U.S. Department of Energy (DOE) Office of Science User Facility operated for the DOE Office of Science by Argonne National Laboratory under Contract No. DE-AC02-06CH11357.

7. References

1. Hamley, I. W. *The Physics of Block Copolymers*; Oxford University Press: New York, **1998**.
2. Abetz, V.; Simon, P. F. W. Phase Behaviour and Morphologies of Block Copolymers. In *Block Copolymers I* (Ed.: V. Abetz); Springer: Berlin, **2005**; pp. 125–212.
3. Park, C.; Yoon, J.; Thomas, E. L. Enabling Nanotechnology with Self Assembled Block Copolymer Patterns. *Polymer* **2003**, *44*, 6725–6760.
4. Guo, C. H.; Lin, Y. H.; Witman, M. D.; Smith, K. A.; Wang, C.; Hexemer, A.; Strzalka, J.; Gomez, E. D.; Verduzco, R. Conjugated Block Copolymer Photovoltaics with Near 3% Efficiency through Microphase Separation. *Nano Lett*. **2013**, *13*, 2957–2963.
5. Chan, E. P.; Walish, J. J.; Urbas, A. M.; Thomas, E. L. Mechanochromic Photonic Gels. *Adv. Mater*. **2013**, *25*, 3934–3947.
6. Boyle, B. M.; French, T. A.; Pearson, R. M.; McCarthy, B. G.; Miyake, G. M. Structural Coloring for Additive Manufacturing: 3D-Printed Photonic Crystals from Block Copolymers. *ACS Nano* **2017**, *11*, 3052–3058.
7. Müller-Buschbaum, P. (Ed.) Forum on Block Copolymers for Nanotechnology Applications. *ACS Appl. Mater. Interfaces* **2017**, *9* 31213–32412.
8. Bates, C. M.; Bates, F. S. Block Polymers — Pure Potential. *Macromolecules* **2017**, *50*, 3–

22.

9. Jinnai, H.; Kaneko, T.; Matsunaga, K.; Abetz, C.; Abetz, V. A Double Helical Structure Formed from an Amorphous, Achiral ABC Triblock Terpolymer. *Soft Matter* **2009**, *5*, 2042–2046.
10. Hajduk, D. A.; Harper, P. E.; Gruner, S. M.; Honeker, C. C.; Kim, G.; Thomas, E. L.; Fetters, L. J. The Gyroid — A New Equilibrium Morphology in Weakly Segregated Diblock Copolymers. *Macromolecules* **1994**, *27*, 4063–4075.
11. Laurer, J. H.; Hajduk, D. A.; Fung, J. C.; Sedat, J. W.; Smith, S. D.; Gruner, S. M.; Agard, D. A.; Spontak, R. J. Microstructural Analysis of a Cubic Bicontinuous Morphology in a Neat SIS Triblock Copolymer. *Macromolecules* **1997**, *30*, 3938–3941.
12. Jinnai, H.; Nishikawa, Y.; Spontak, R. J.; Smith, S. D.; Agard, D. A.; Hashimoto, T. Direct Measurement of Interfacial Curvature Distributions in a Bicontinuous Block Copolymer Morphology. *Phys. Rev. Lett.* **2000**, *84*, 518–521.
13. Tyler, C. A.; Morse, D. C. Orthorhombic *Fddd* Network in Triblock and Diblock Copolymer Melts. *Phys. Rev. Lett*. **2005**, *94*, 208302.
14. Takenaka, M.; Wakada, T.; Akasaka, S.; Nishitsuji, S.; Saijo, K.; Shimizu, H.; Kim, M. I.; Hasegawa, H. Orthorhombic *Fddd* Network in Diblock Copolymer Melts. *Macromolecules* **2007**, *40*, 4399–4402.
15. Lee, S.; Bluemle, M. J.; Bates, F. S. Discovery of a Frank-Kasper σ Phase in Sphere-Forming Block Copolymer Melts. *Science* **2010**, *330*, 349–353.
16. Drobny, J. G. *Handbook of Thermoplastic Elastomers*, 2nd ed.; Elsevier: Oxford, **2014**.
17. Hamersky, M. W.; Smith, S. D.; Gozen, A. O.; Spontak, R. J. Phase Behavior of Triblock Copolymers Varying in Molecular Asymmetry. *Phys. Rev. Lett*. **2005**, *95*, 168306.
18. Watanabe, H. Slow Dielectric-Relaxation of a Styrene-Isoprene-Styrene Triblock Copolymer with Dipole Inversion in the Middle Block – A Challenge to a Loop-Bridge Problem. *Macromolecules* **1995**, *28*, 5006–5011.
19. Karatasos, K.; Anastasiadis, S. H.; Pakula, T.; Watanabe, H. On the Loops-to-Bridges Ratio in Ordered Triblock Copolymers: An Investigation by Dielectric Relaxation Spectroscopy

and Computer Simulations. *Macromolecules* **2000**, *33*, 523–541.

20. Watanabe, H.; Sato, T.; Osaki, K. Concentration Dependence of Loop Fraction in Styrene-Isoprene-Styrene Triblock Copolymer Solutions and Corresponding Changes in Equilibrium Elasticity. *Macromolecules* **2000**, *33*, 2545–2550.
21. Kane, L.; Norman, D. A.; White, S. A.; Matsen, M. W.; Satkowski, M. M.; Smith, S. D.; Spontak, R. J. Molecular, Nanostructural and Mechanical Characteristics of Lamellar Triblock Copolymer Blends: Effects of Molecular Weight and Constraint. *Macromol. Rapid Commun.* **2001**, *22*, 281–296.
22. Matsen, M. W.; Schick, M. Lamellar Phase of a Symmetrical Triblock Copolymer. *Macromolecules* **1994**, *27*, 187–192.
23. Matsen, M. W.; Thompson, R. B. Equilibrium Behavior of Symmetric ABA Triblock Copolymer Melts. *J. Chem. Phys.* **1999**, *111*, 7139–7146.
24. Tallury, S. A.; Mineart, K. P.; Woloszczuk, S.; Williams, D. N.; Thompson, R. B.; Pasquinelli, M. A.; Banaszak, M.; Spontak, R. J. Molecular-Level Insights into Asymmetric Triblock Copolymers: Network and Phase Development. *J. Chem. Phys.* **2014**, *141*, 121103.
25. Tallury, S. S.; Spontak, R. J.; Pasquinelli, M. A. Dissipative Particle Dynamics of Triblock Copolymer Melts: A Midblock Conformational Study at Moderate Segregation. *J. Chem. Phys.* **2014**, *141*, 244911.
26. Fredrickson, G. H.; Milner, S. T.; Leibler, L. Multicritical Phenomena and Microphase Ordering in Random Block Copolymer Melts. *Macromolecules* **1992**, *25*, 6341–6354.
27. Park, C. H.; Lee, C. H.; Guiver, M. D.; Lee, Y. M. Sulfonated Hydrocarbon Membranes for Medium-Temperature and Low-Humidity Proton Exchange Membrane Fuel Cells (PEMFCs). *Prog. Polym. Sci*. **2011**, *36*, 1443–1498.
28. Denisova, Y. I.; Gringolts, M. L.; Krentsel, L. B.; Shandryuk, G. A.; Peregudov, A. S.; Finkelshtein, E. S.; Kudryavtsev, Y. V. *Polym. Sci. Ser. B* **2017**, *59*, 412–420.
29. Spontak, R. J.; Smith, S. D.; Satkowski, M. M.; Ashraf, A.; Zielinski, J. M. Synthesis and Morphological Studies of $(AB)_n$ Multiblock Copolymers. In Polymer Solutions, Blends, and Interfaces (Eds: I. Noda and D. N. Rubingh), Elsevier: Amsterdam, **1992**, pp. 65–88.

30. Smith, S. D.; Spontak, R. J.; Satkowski, M. M.; Ashraf, A.; Lin, J. S. Microdomain Contraction in Microphase-Separated Multiblock Copolymers. *Phys. Rev. B* **1993**, *47*, 14555–14558.

31. Smith, S. D.; Spontak, R. J.; Satkowski, M. M.; Ashraf, A.; Heape, A. K.; Lin, J. S. Microphase-Separated Poly(styrene-*b*-isoprene)$_n$ Multiblock Copolymers with Constant Block Lengths. *Polymer* **1994**, *35*, 4527–4536.

32. Spontak, R. J.; Smith, S. D. Perfectly-Alternating Linear (AB)$_n$ Multiblock Copolymers: Effect of Molecular Design on Morphologies and Properties. *J. Polym. Sci. B: Polym. Phys.* **2001**, *39*, 947–955.

33. Wu, L. F.; Cochran, E. W.; Lodge, T. P.; Bates, F. S. Consequences of Block Number on the Order-Disorder Transition and Viscoelastic Properties of Linear (AB)$_n$ Multiblock Copolymers. *Macromolecules* **2004**, *37*, 3360–3368.

34. Lee, I.; Bates, F. S. Synthesis, Structure, and Properties of Alternating and Random Poly(styrene-*b*-butadiene) Multiblock Copolymers. *Macromolecules* **2013**, *46*, 4529–4539.

35. Eagan, J. M.; Xu, J.; Di Girolamo, R.; Thurber, C. M.; Macosko, C. W.; LaPointe, A. M.; Bates, F. S.; Coates, G. W. Combining Polyethylene and Polypropylene: Enhanced Performance with PE/iPP Multiblock Polymers. *Science* **2017**, *355*, 814–816.

36. Bates, F. S.; Hillmyer, M. A.; Lodge, T. P.; Bates, C. M.; Delaney, K. T.; Fredrickson, G. H. Multiblock Polymers: Panacea or Pandora's Box? *Science* **2012**, *336*, 434–440.

37. Winey, K. I.; Thomas, E. L.; Fetters, L. J. Isothermal Morphology Diagrams for Binary Blends of Diblock Copolymer and Homopolymer. *Macromolecules* **1992**, *25*, 2645–2650.

38. Matsen, M. W. Phase-Behavior of Block-Copolymer Homopolymer Blends. *Macromolecules* **1995**, *28*, 5765–5773.

39. Spontak, R. J.; Patel, N. P. Phase Behavior of Block Copolymer Blends. In: *Block Copolymer Science and Technology*, (Ed: I. W. Hamley), Wiley: New York, **2004**, pp. 159–212.

40. Krishnan, A. S.; Smith, S. D.; Spontak, R. J. Ternary Phase Behavior of a Triblock Copolymer in the Presence of an Endblock-Selective Homopolymer and a Midblock-

Selective Oil. *Macromolecules* **2012**, *45*, 6056–6067.

41. Lodge, T. P.; Pudil, B.; Hanley, K. J. The Full Phase Behavior for Block Copolymers in Solvents of Varying Selectivity. *Macromolecules* **2002**, *35*, 4707–4717.
42. Woloszczuk, S.; Tuhin, M. O.; Gade, S. R.; Pasquinelli, M. A.; Banaszak, M.; Spontak, R. J. Complex Phase Behavior and Network Characteristics of Midblock-Solvated Triblock Copolymers as Physically-Crosslinked Soft Materials. *ACS Appl. Mater. Interfaces* **2017**, *9*, 39940–39944.
43. Shankar, R.; Ghosh, T. K.; Spontak, R. J. Electroactive Nanostructured Polymers as Tunable Actuators. *Adv. Mater.* **2007**, *19*, 2218–2223.
44. Shankar, R.; Ghosh, T. K.; Spontak, R. J. Dielectric Elastomers as Next-Generation Polymeric Actuators. *Soft Matter* **2007**, *3*, 1116–1129.
45. Kim, B.; Park, Y. D.; Min, K.; Lee, J. H.; Hwang, S. S.; Hong, S. M.; Kim, B. H.; Kim, S. O.; Koo, C. M. Electric Actuation of Nanostructured Thermoplastic Elastomer Gels with Ultralarge Electrostriction Coefficients. *Adv. Funct. Mater*. **2011**, *21*, 3242–3249.
46. Vargantwar, P. H.; Ozcam, A. E.; Ghosh, T. K.; Spontak, R. J. Prestrain-Free Dielectric Elastomers Based on Acrylic Thermoplastic Elastomer Gels: A Morphological and (Electro)Mechanical Property Study. *Adv. Funct. Mater*. **2012**, *22*, 2100–2113.
47. Armstrong, D. P.; Spontak, R. J. Designing Dielectric Elastomers over Multiple Length Scales for 21st-Century Soft Materials Technologies. *Rubber Chem. Technol*. **2017**, *90*, 207–224.
48. Song, S.; Feng, J.; Wu, P. A New Strategy to Prepare Polymer-based Shape Memory Elastomers. *Macromol. Rapid Commun.* **2011**, *32*, 1569–1575.
49. Zhang, Q.; Song, S.; Feng, J.; Wu, P. A New Strategy to Prepare Polymer Composites with Versatile Shape Memory Properties. *J. Mater. Chem.* **2012**, *22*, 24776–24782.
50. Mineart, K. P.; Tallury, S. S.; Li, T.; Lee, B.; Spontak, R. J. Phase-Change Thermoplastic Elastomer Blends for Tunable Shape Memory by Physical Design. *Ind. Eng. Chem. Res.* **2016**, *55*, 12590–12597.
51. Creton, C.; Hu, G. J.; Deplace, F.; Morgret, L.; Shull, K. R. Large-Strain Mechanical

Behavior of Model Block Copolymer Adhesives. *Macromolecules* **2009**, *42*, 7605–7615.

52. Sudarsan, A. P.; Wang, J.; Ugaz, V. M. Thermoplastic Elastomer Gels: An Advanced Substrate for Microfluidic Chemical Analysis Systems. *Anal. Chem*. **2005**, *77*, 5167–5173.

53. Mineart, K. P.; Lin, Y.; Desai, S. C.; Krishnan, A. S.; Spontak, R. J.; Dickey, M. D. Ultrastretchable, Cyclable and Recyclable 1- and 2-Dimensional Conductors Based on Physically Cross-Linked Thermoplastic Elastomer Gels. *Soft Matter* **2013**, *9*, 7695–7700.

54. Alexandridis, P.; Olsson, U.; Lindman, B. A Record Nine Different Phases (Four Cubic, Two Hexagonal, and One Lamellar Lyotropic Liquid Crystalline and Two Micellar Solutions) in a Ternary Isothermal System of an Amphiphilic Block Copolymer and Selective Solvents (Water And Oil). *Langmuir* **1998**, *14*, 2627–2638.

55. He, Y. Y.; Boswell, P. G.; Buhlmann, P.; Lodge, T. P. Ion Gels by Self-Assembly of a Triblock Copolymer in an Ionic Liquid. *J. Phys. Chem. B* **2007**, *111*, 4645–4652.

56. Shen, W.; Zhang, K .C.; Kornfield, J. A.; Tirrell, D. A. Tuning the Erosion Rate of Artificial Protein Hydrogels through Control of Network Topology. *Nat. Mater.* **2006**, *5*, 153–158.

57. Hallinan, D. T.; Balsara, N. P. Polymer Electrolytes. *Ann. Rev. Mater. Res*. **2013**, *43*, 503–525.

58. Vargantwar, P. H.; Roskov, K. E.; Ghosh, T. K.; Spontak, R. J. Enhanced Biomimetic Performance of Ionic Polymer–Metal Composite Actuators Prepared with Nanostructured Block Ionomers. *Macromol. Rapid Commun.* **2012**, *33*, 61–68.

59. Al-Mohsin, H. A.; Mineart, K. P.; Spontak, R. J. Highly Flexible Aqueous Photovoltaic Elastomer Gels Derived from Sulfonated Block Ionomers. *Adv. Energy Mat.* **2015**, *8*, 1401941.

60. Al-Mohsin, H. A.; Mineart, K. P.; Armstrong, D. P.; El-Shafei, A.; Spontak, R. J. Quasi-Solid-State Dye-Sensitized Solar Cells Containing a Charged Thermoplastic Elastomeric Gel Electrolyte and Hydrophilic/phobic Photosensitizers. *Sol. RRL* **2018**, 1700145.

61. Geise, G. M.; Freeman, B. D.; Paul, D. R. Characterization of a Sulfonated Pentablock Copolymer for Desalination Applications. *Polymer* **2010**, *51*, 5815–5822.

62. Fan, Y.; Zhang, M.; Moore, R. B.; Cornelius, C. J. Structure, Physical Properties, and

Molecule Transport of Gas, Liquid, and Ions within a Pentablock Copolymer. *J. Membr. Sci.* **2014**, *464*, 179−187.

63. Ansaloni, L.; Dai, Z.; Ryan, J. J.; Mineart, K. P.; Saud, K. T.; Yu, Q.; Hägg, M.-B.; Spontak, R. J.; Deng, L. Base- and Acid-Gas Transport through Solvent-Templated Block Ionomers: Effect of Humidity on Ammonia and Carbon Dioxide Permeation. *Adv. Mater. Interfaces* **2017**, 1700854.
64. Shankar, R.; Krishnan, A. S.; Ghosh, T. K.; Spontak, R. J. Triblock Copolymer Organogels as High-Performance Dielectric Elastomers. *Macromolecules* **2008**, *41*, 6100−6109.
65. Armstrong, D. P.; Mineart, K. P.; Lee, B.; Spontak, R. J. Olefinic Thermoplastic Elastomer Gels: Combining Polymer Crystallization and Microphase Separation in a Selective Solvent. *ACS Macro Lett*. **2016**, *5*, 1273−1277.
66. Ashraf, A.; Ryan, J. J.; Satkowski, M. M.; Smith, S. D.; Spontak, R. J. Effect of Systematic Hydrogenation on the Phase Behavior and Nanostructural Dimensions of Block Copolymers. *ACS Appl. Mater. Interfaces* **2018**, *10*, 3186−3190.
67. Qian, H.; Lu, Z.; Chen, L.; Li, Z.; Sun, C. Computer Simulation of Cyclic Block Copolymer Microphase Separation. *Macromolecules* **2005**, *38*, 1395−1401.
68. Groot, R. D.; Madden, T. J.; Tildesley, D. J. On the Role of Hydrodynamic Interactions in Block Copolymer Microphase Separation. *J. Chem. Phys.* **1999**, *110*, 9739−9749.
69. Plimpton, S. Fast Parallel Algorithms for Short-Range Molecular-Dynamics. *J. Comput. Phys*. **1995**, *117*, 1−19.
70. Matsen, M. W. Effect of Architecture on the Phase Behavior of AB-Type Block Copolymer Melts. *Macromolecules* **2012**, *45*, 2161–2165.
71. Semenov, A. N. Theory of Block-Copolymer Interfaces in the Strong Segregation Limit. *Macromolecules* **1993**, *26*, 6617–6621.
72. Kleppinger, R.; Mischenko, N.; Theunissen, E.; Reynaers, H. L.; Koch, M. H. J.; Almdal, K.; Mortensen, K. Shear-Induced Single Crystalline Mesophases in Physical Networks of Gel-Forming Triblock Copolymer Solutions. *Macromolecules* **1997**, *30*, 7012–7014.
73. Mortensen, K.; Theunissen, E.; Kleppinger, R.; Almdal, K.; Reynaers, H. Shear-Induced

Morphologies of Cubic Ordered Block Copolymer Micellar Networks Studied by in Situ Small-Angle Neutron Scattering and Rheology. *Macromolecules* **2002**, *35*, 7773–7781.

74. Krishnan, A. S.; van Zanten, J. H.; Seifert, S.; Lee, B.; Spontak, R. J. Selectively-Solvated Triblock Copolymer Networks under Biaxial Strain. *Appl. Phys. Lett*. **2011**, *99*, 101908.
75. Park, M. J.; Bang, J.; Harada, T.; Char, K.; Lodge, T. P. Epitaxial Transitions among FCC, HCP, BCC, and Cylinder Phases in a Block Copolymer Solution. *Macromolecules* **2004**, *37*, 9064–9075.
76. Bang, J.; Lodge, T. P. On the Selection of FCC and BCC Lattices in Poly(styrene-b-isoprene) Copolymer Micelles. *Macromol. Res*. **2008**, *16*, 51–56.
77. Senesi, A. J.; Lee, B. Small-Angle Scattering of Particle Assemblies. *J. Appl. Crystallog.* **2015**, *48*, 1172–1182.
78. Chantawansri, T. L.; Sirk, T. W.; Sliozberg, Y. R. Entangled Triblock Copolymer Gel: Morphological and Mechanical Properties. *J. Chem. Phys*. **2013**, *138*, 024908.
79. Li, S.; Chen, J.; Xu, D.; Shi, T. Topological Constraints of Network Chains in Telechelic Associative Polymer Gels. *J. Chem. Phys*. **2015**, *143*, 244902.
80. Zhong, M.; Wang, R.; Kawamoto, K.; Olsen, B. D.; Johnson, J. A. Quantifying the Impact of Molecular Defects on Polymer Network Elasticity. *Science* **2016**, *353*, 1264–1268.
81. Bras, R. E.; Shull, K. R. Self-Consistent Field Theory of Gelation in Triblock Copolymer Solutions. *Macromolecules* **2009**, *42*, 8513–8520.
82. Zhang, Q.; Lin, J.; Wang, L.; Xu, Z. Theoretical Modeling and Simulations of Self-Assembly of Copolymers in Solution. *Prog. Polym. Sci*. **2017**, *75*, 1–30.